Proceedings of the 2020 28th Conference on Nuclear Engineering

Joint With the ASME 2020 Power Conference

ICONE28-POWER2020

August 2-6, 2020, Anaheim, California, USA

ICONE28-POWER2020-6524

A COMPARATIVE STUDY OF CONSTRAINED AND UNCONSTRAINED MELTING INSIDE A SPHERE

Rohit Kothari[1]

Discipline of Mechanical Engineering, Indian Institute of Technology Indore, Simrol, Indore 453552, India

School of Nuclear Engineering, Purdue University, West Lafayette, IN 47907, USA

Shripad T. Revankar

School of Nuclear Engineering, Purdue University, West Lafayette, IN 47907, USA

Division of Advanced Nuclear Engineering, POSTECH, Pohang 790-784, Republic of Korea

Santosh K. Sahu, Shailesh I. Kundalwal

Discipline of Mechanical Engineering, Indian Institute of Technology Indore, Simrol, Indore 453552, India

ABSTRACT

Present study is focused on the computational analysis of melting of PCM inside the spherical capsule. Both unconstrained and constrained melting is analyzed for the constant PCM volume and similar initial and boundary conditions. RT27 is chosen as the PCM for this study. Air is considered at the top of PCM inside the spherical capsule. Results are validated with the existing experimental and computational results and found to be in good agreement. Results obtained from present study are compared for the melting fraction, pattern and time. Composite diagrams are presented for the streamline and temperature contours.

Keywords: Phase change materials, Unconstrained, Constrained, Spherical capsule, CFD.

NOMENCLATURE

c_p	Constant pressure specific heat, J/kg-K
C	Porosity constant, kg/m^3-s
D_i	Inner diameter of spherical capsule, m
g	Gravitational acceleration, m^2/s
H	Total enthalpy, J/kg
k	Thermal conductivity, W/m-K
L	Latent heat of fusion, J/kg
P	Pressure, Pa
r	Coordinate, m
R_i	Inner radius of spherical capsule, m
R_o	Outer radius of spherical capsule, m
S	Source term
t	Time, s
t_w	Thickness of shell, m
T	Temperature of PCM, K
T_o	Initial temperature of PCM, K
v_r	Radial velocity component, m/s
v_θ	Polar velocity component, m/s
x, y	Coordinate, m

Greek symbols

α	Thermal diffusivity, m^2/s
β	Thermal expansion coefficient, 1/K
λ	Liquid volume fraction
ε	Small computational constant
θ	Coordinate, rad
μ	Dynamic viscosity, Pa-s
ν	Kinematic viscosity, m^2/s
ρ	Density, kg/m^3

[1] Contact author: rohitkothari2892@gmail.com

φ	Volume fraction of liquid PCM in a computational cell
Subscripts	
i, j	Components
l	Liquid
liquidus	Above melting point
m	Melting
PCM	Phase change material
ref	Reference point
solidus	Before melting point
w	Wall

1. INTRODUCTION

Phase change heat storage systems have been widely used in various applications such as waste heat recovery, solar energy, air heating, medical and central air conditioning applications. The use of phase change materials (PCMs) in these applications is an effectual way to enhance the utilization and conservation of energy. In general, PCMs are encapsulated in containers for better use. Different shapes of containers were used to encapsulate the PCMs such as rectangular, cylindrical, spherical and elliptical. Spherical containers are most widely suitable for encapsulating the PCM due to its effortless packing in the heat storage system and high heat transfer surface area to volume ratio.

Wide varieties of studies are performed to investigate the melting and solidification of PCM [1-17]. Studies on melting of PCM inside the spherical containers are divided into two categories such as unconstrained [1-10] and constrained melting [11-15]. PCM filled spherical capsule is externally heated in both the cases. In case of unconstrained melting the unmelted solid PCM is free to move and sinks down at the bottom of capsule. This happens due to density difference between the solid and liquid PCM. The melting at the bottom of the capsule occurs as the close contact melting. Conduction is dominant mode of heat transfer at the bottom of the capsule in unconstrained melting. However, a tube or thermocouple rod is inserted in the middle of the capsule in case of constrained melting. The tube/rod holds the solid PCM and doesn't allow it to sink at the bottom. Therefore, no close contact melting occurs in constrained melting and natural convection is dominant mode of heat transfer at the bottom.

Assis et al. [1] carried out experimental and numerical investigation on the unconstrained melting of PCM inside the spherical capsule. RT27 has been used as the PCM. Air region is provided at the top of PCM region to accommodate the volume expansion of the PCM. Effects of various geometrical and thermal parameters are investigated. Archibold et al. [5, 6] performed numerical investigation for unconstrained melting of high temperature PCM inside the spherical capsule. High temperature phase change material ($NaNo_3$) has been chosen as the PCM. Correlations have been performed for melt fraction in terms of dimensionless numbers such as Fourier, Stefan and Grashof numbers. Tan et al. [11] carried out experimental and numerical investigation on the constrained melting of PCM. N-octadecane is chosen as the PCM. Unstable flow structure and waviness at the bottom of the PCM is reported in their study. Li et al. [13] performed experimental and numerical investigation to analyze the constrained melting of PCM inside the spherical capsule. Inner radius and thickness of the capsule have been kept as 40 mm and 2 mm, respectively. Paraffin wax has been used as the PCM. The effects of various parameters such as thermal expansion coefficient of PCM, radius, material and outer wall temperature of the PCM capsule have been examined in detail. Experimental and numerical investigation on constrained melting of PCM is also performed by Fan et al. [14]. Internal circumferential fins are inserted horizontally inside the spherical capsule and parametric investigations are performed by varying the fin heights.

It is evident from the literature that various studies are reported on the unconstrained and constrained melting of PCM. Reported studies are available to investigate the thermal and geometrical parameters and melting pattern of PCM inside the spherical capsule. However, the focus of the present study is to compare unconstrained and constrained melting of PCM inside the spherical capsule as this is not significantly explored in the literature. Therefore in this study, unconstrained and constrained melting with air region at the top is considered. Constant volume of PCM and similar boundary condition are taken for the present investigation. Melting time and melt fraction is compared for both the cases. Composite diagrams are presented for temperature contours, melting pattern and streamline contours.

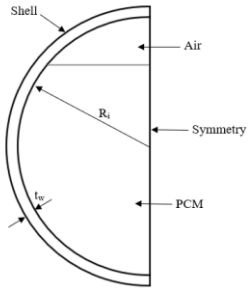

FIGURE 1: SCHEMATIC DIAGRAM OF THE COMPUTATIONAL DOMAIN

TABLE 1: THERMOPHYSICAL PROPERTIES OF PCM

Properties (unit)	RT27
Density (kg/m^3)	870 (Solid), 760 (Liquid at 30^{o}C)
Dynamic viscosity (kg/m-s)	3.42×10^{-3}
Latent heat of fusion (kJ/kg)	179
Melting temperature (^{o}C)	28 (Solidus), 30 (Liquidus)
Specific heat (kJ/kg-K)	2.4 (Solid), 1.8 (Liquid)

Thermal expansion coefficient (1/K)	0.5×10^{-3}
Thermal conductivity (W/m-K)	0.24Solid), 0.15 (Liquid)

2. PHYSICAL AND MATHEMATICAL MODEL

In this study a spherical glass container is used to encapsulate the PCM. The geometry considered in the present study is similar as taken by Assis et al. [1] in their experimental and numerical investigation. The schematic diagram of computational domain is shown in Fig. 1(a) for case I and II and Fig. 1(b) for case III, considering the symmetry of the geometry. 15% of volume of sphere is filled with air in cases I and III. RT27 is chosen as the PCM in this study and its thermophysical properties are shown in Table 1. Here, two dimensional transient numerical simulations are performed using Ansys Fluent 19.2 software. Various assumptions are made during this study such as isotropic and homogeneous phases of PCM, incompressible, unsteady and laminar flow, neglecting viscous dissipation. Two different cases are considered in present study as shown in Table 2. Constant volume of PCM is taken for both the cases. Axisymmetric modelling has been considered for the present investigation.

TABLE 2: VARIOUS CASES CONSIDERED IN THIS STUDY

Cases	Type of melting	Geometry	Density variations
I	Unconstrained	Air region at the top of PCM inside the spherical capsule	Constant density in solid phase and linearly varying density in mushy/liquid region
II	Constrained	Air region at the top of PCM inside the spherical capsule.	Boussinesq approximation

For unconstrained melting

Continuity:

$$\frac{\partial \rho}{\partial t}+\frac{1}{r^2}\frac{\partial}{\partial r}(\rho v_r r^2)+\frac{1}{r\sin\theta}\frac{\partial}{\partial \theta}(\rho v_\theta \sin\theta)=0 \quad (1)$$

Momentum in radial direction:

$$\frac{\partial(\rho v_r)}{\partial t}+\frac{1}{r^2}\frac{\partial}{\partial r}\left(\rho v_\theta r^2 v_r\right)+\frac{1}{r\sin\theta}\frac{\partial}{\partial \theta}\left(\rho v_\theta \sin\theta v_r\right)-\frac{\rho v_\theta^2}{r}$$

$$=-\frac{\partial P}{\partial r}+\mu\left[\nabla^2(\rho v_r)-\frac{2\rho v_r}{r^2}-\frac{2}{r^2}\frac{\partial(\rho v_\theta)}{\partial \theta}-\frac{2\rho v_\theta \cot\theta}{r^2}\right] \quad (2a)$$

$$+\rho g_r \beta(T-T_m)+S_i$$

Momentum in Polar direction:

$$\frac{\partial(\rho v_\theta)}{\partial t}+\frac{1}{r^2}\frac{\partial}{\partial r}\left(\rho v_r r^2 v_\theta\right)+\frac{1}{r\sin\theta}\frac{\partial}{\partial \theta}\left(\rho v_\theta \sin\theta v_\theta\right)+\frac{\rho v_r v_\theta}{r}$$

$$=-\frac{1}{r}\frac{\partial P}{\partial \theta}+\mu\left[\nabla^2(\rho v_r)+\frac{2}{r^2}\frac{\partial(\rho v_r)}{\partial \theta}-\frac{2\rho v_\theta}{r^2\sin^2\theta}\right] \quad (2b)$$

$$+\rho g_r \beta(T-T_m)+S_i$$

Energy Equation:

$$\frac{\partial(\rho h)}{\partial t}+\frac{1}{r^2}\frac{\partial}{\partial r}\left(\rho r^2 v_r h\right)+\frac{1}{r\sin\theta}\frac{\partial}{\partial \theta}\left(\rho v_\theta \sin\theta h\right)$$

$$=\frac{k}{c_p}\nabla^2 h-\frac{1}{c_p}\frac{\partial \lambda}{\partial t}-\frac{1}{r^2}\frac{\partial}{\partial r}\left(\rho r^2 v_r \lambda\right)+\frac{1}{r\sin\theta}\frac{\partial}{\partial \theta}\left(\rho v_\theta \lambda \sin\theta\right) \quad (3)$$

For constrained melting

Continuity:

$$\frac{\partial \rho}{\partial t}+\frac{1}{r^2}\frac{\partial}{\partial r}(\rho v_r r^2)+\frac{1}{r\sin\theta}\frac{\partial}{\partial \theta}(\rho v_\theta \sin\theta)=0 \quad (4)$$

Momentum in radial direction:

$$\frac{\partial(\rho v_r)}{\partial t}+\frac{1}{r^2}\frac{\partial}{\partial r}\left(\rho v_\theta r^2 v_r\right)+\frac{1}{r\sin\theta}\frac{\partial}{\partial \theta}\left(\rho v_\theta \sin\theta v_r\right)-\frac{\rho v_\theta^2}{r}$$

$$=-\frac{\partial P}{\partial r}+\mu\left[\nabla^2(\rho v_r)-\frac{2\rho v_r}{r^2}-\frac{2}{r^2}\frac{\partial(\rho v_\theta)}{\partial \theta}-\frac{2\rho v_\theta \cot\theta}{r^2}\right] \quad (5a)$$

$$+\rho g_r \beta(T-T_m)+S_i$$

Momentum in Polar direction:

$$\frac{\partial(\rho v_\theta)}{\partial t}+\frac{1}{r^2}\frac{\partial}{\partial r}\left(\rho v_r r^2 v_\theta\right)+\frac{1}{r\sin\theta}\frac{\partial}{\partial\theta}\left(\rho v_\theta \sin\theta v_\theta\right)+\frac{\rho v_r v_\theta}{r}$$

$$=-\frac{1}{r}\frac{\partial P}{\partial\theta}+\mu\left[\nabla^2(\rho v_r)+\frac{2}{r^2}\frac{\partial(\rho v_r)}{\partial\theta}-\frac{2\rho v_\theta}{r^2\sin^2\theta}\right] \quad (5b)$$

$$+\rho g_r\beta\left(T-T_m\right)+S_i$$

Energy Equation:

$$\frac{\partial(\rho h)}{\partial t}+\frac{1}{r^2}\frac{\partial}{\partial r}\left(\rho r^2 v_r h\right)+\frac{1}{r\sin\theta}\frac{\partial}{\partial\theta}\left(\rho v_\theta \sin\theta h\right)$$

$$=\frac{k}{c_p}\nabla^2 h-\frac{1}{c_p}\frac{\partial\lambda}{\partial t}-\frac{1}{r^2}\frac{\partial}{\partial r}\left(\rho r^2 v_r\lambda\right)+\frac{1}{r\sin\theta}\frac{\partial}{\partial\theta}\left(\rho v_\theta\lambda\sin\theta\right) \quad (6)$$

Here, ∇ is a Laplace operator and is defined as:

$$\nabla^2=\frac{1}{r^2}\frac{\partial}{\partial r}\left(r^2\frac{\partial}{\partial r}\right)+\frac{1}{r^2\sin\theta}\frac{\partial}{\partial\theta}\left(\sin\theta\frac{\partial}{\partial\theta}\right) \quad (7)$$

Initial and Boundary conditions:

$$v_r(r,\theta,0)=v_\theta(r,\theta,0)=0\,,\ T(r,\theta,0)=T_o \quad (8a)$$

$$T(R_o,\theta,t)=T_w \quad (8b)$$

$$k_w\left.\frac{\partial T_w}{\partial r}\right|_{r=R_i}=k_{pcm}\left.\frac{\partial T_{pcm}}{\partial r}\right|_{r=R_i} \quad (8c)$$

$$v_r(R_i,\theta,t)=v_\theta(R_i,\theta,t)=0 \quad (8d)$$

where

$$\mathrm{H}=h+\lambda \quad (9)$$

h and λ are sensible enthalpy and latent heat of fusion, respectively and are defined as:

$$h=h_{ref}+\int_{T_{ref}}^{T}c_p dT \quad (10)$$

where h_{ref} and T_{ref} are reference sensible heat and temperature, respectively.

$$\lambda=\varphi L \quad (11)$$

Here, L is the latent heat and φ is the volume fraction of liquid PCM of a computational cell in which the phase transition is taking place ($0<\varphi<1$). φ is defined as:

$\varphi=0$	$T < T_{solidus}$	Solid	
$0<\varphi<0$	$T_{solidus} < T < T_{liquidus}$	Mushy	(12)
$\varphi=1$	$T < T_{liquidus}$	Liquid	

Here, solid liquid interface is tracked with the help of enthalpy-porosity technique introduced by Voller and Prakash [18] and Brent et al. [19]. This method introduces a source term in the momentum equation and is given by:

$$S_i=-A(\varphi)v\,, \quad (13)$$

where v is v_r or v_θ for radial and polar momentum equation in axisymmetric melting. While, v is taken as v_i for symmetric melting.

Here, the porosity function $A(\varphi)$ is given by Brent et al. [19] and expressed as:

$$A(\varphi)=\frac{C(1-\varphi)^2}{\varphi^3+\varepsilon} \quad (14)$$

Here, ε is a small computational constant and its value is taken as ε = 0.001. C is a mushy zone constant and the value of C is taken as 10^5 [1].

3. COMPUTATIONAL PROCEDURE

PISO method is used in Ansys Fluent 19.2 software to solve the governing equations [20]. The under relaxation factors used for pressure, density and body force is considered as 0.5, while it is taken as 0.2 for momentum and liquid faction and 0.8 for energy. The convergence criteria for continuity, momentum and energy equation is chosen as 10^{-5}, 10^{-5} and 10^{-8}, respectively. After grid and time independent studies, 7554 grid cells and 0.005 s have been chosen to simulate both the cases in the present study.

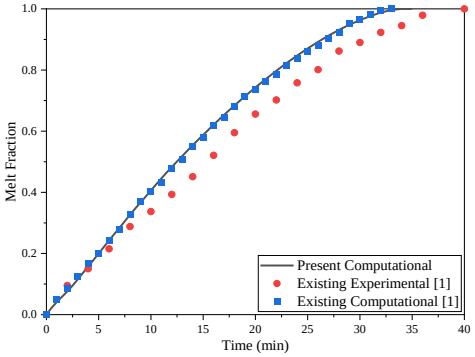

(A)

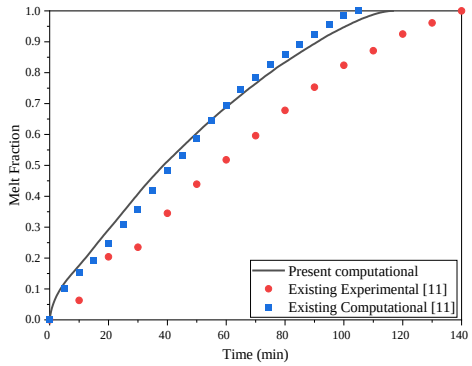

(B)

FIGURE 2: COMPARISON OF MELT FRACTION OBTAINED FROM PRESENT COMPUTATIONAL STUDY FOR (A) UNCONSTRAINED, (B) CONSTRAINED MELTING WITH EXISTING EXPERIMENTAL/COMPUTATIONAL STUDIES

4. VALIDATION

Here, present model is validate with the existing experimental and numerical investigation for both unconstrained and constrained melting and are shown in Fig. 2(A) and 2(B), respectively. Unconstrained melting is validated with the experimental and numerical results obtained by Assis et al. [1], while the constrained melting is validated against the results of Tan et al. [11]. It may be noted that the present model agrees well with the existing results.

5. RESULTS AND DISCUSSION

In this study, numerical simulations are performed for RT27 filled spherical glass capsule. The inner radii and thickness of the capsule is 40 mm and 2 mm, respectively. Unconstrained and constrained melting with air region at the top are investigated in this study. CFD simulations are performed for constant volume of PCM in each case. Initial temperature of the entire system is maintained at 23^{o}C and the temperature at the walls of the capsule is maintained 10^{o}C higher than the mean melting temperature of the PCM.

Fig. 3 shows the melting pattern of the PCM inside the spherical capsule for different time instants such as 5, 10, 15, 20 and 25 mins. It may be noted from the figure that in both the cases the thin layer of liquid PCM is formed at the bottom during the early stages of melting. This can be clearly seen from melting pattern shown after 5 min. This happens due to low value of subcooling of PCM. Here, the melting of PCM occurs due to transfer of heat from bottom of the capsule to PCM through conduction. With the progress of melting process, the thin liquid layer continues to grow in both the cases. Subsequently, hot liquid PCM from the bottom starts moving upwards due to strong natural convection, which forces the cold liquid PCM downwards. This increases the melting rate at the top of the capsule as can be seen form the figure. In case of unconstrained melting the natural convection forces the solid PCM downwards and squeezes the liquid layer formed at the bottom of the capsule. Therefore, the melting at the bottom of the capsule in case of unconstrained melting occurs due to conduction dominated heat transfer. While, it is always convection dominated from the side and top of the capsule. In case of constrained melting as the rod/tube at the center of the capsule holds the solid PCM and therefore, the liquid PCM present at the top of the capsule is not able to push the solid PCM. Therefore, the liquid layer at the bottom continues to grow and melting is convection dominated from all the sides in case of constrained melting.

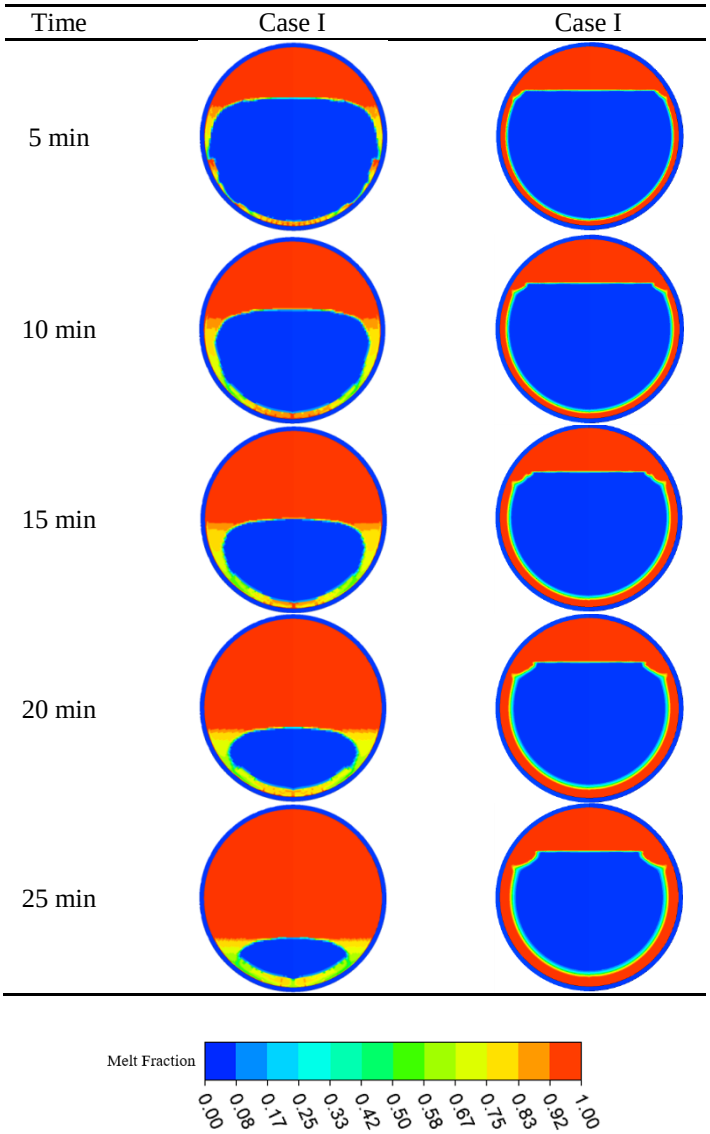

FIGURE 3: MELTING PATTERN OF PCM FOR DIFFERENT CASES

Fig. 4 shows the melting fraction of PCM at different time duration. It can be seen that the melting of PCM is faster in case of unconstrained melting compared to constrained melting. This is because the solid PCM does not fully contribute in the melting process in case of constrained

melting and remain adhered to the rod/tube. However, the solid PCM sink at the bottom of the capsule and continue to take part in melting process. It has been reported that the melting time of PCM for the same PCM volume, initial and boundary conditions is 32 min and 220 min, respectively in case of unconstrained and constrained melting.

Linear density variation and Boussinesq approximations are assumed for unconstrained and constrained melting, respectively. Effect of these density variations can be seen from Fig. 5, which shows the composite diagram containing temperature and velocity contours. It can be seen that in case of unconstrained melting because of the linear density variation, PCM expands and the air region gets compressed. This is more closer to the real unconstrained melting of PCM. However, in case of constrained melting, because of Boussinesq approximation, the expansion of PCM is negligible and the volume of air region remains constant. Also, it can be seen from Fig. 5 that temperature contours are more concentric in case of constrained melting compared to unconstrained melting. However, the rate of increase of temperature is greater in unconstrained melting, which is advantageous in the applications where quick melting is required.

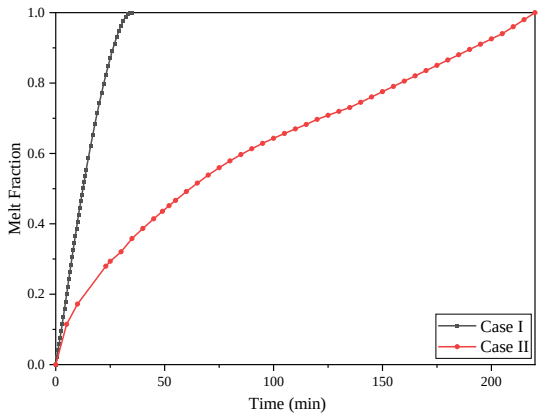

FIGURE 4: MELT FRACTION OF PCM OBTAINED FROM PRESENT COMPUTATIONAL STUDY FOR DIFFERENT CASES

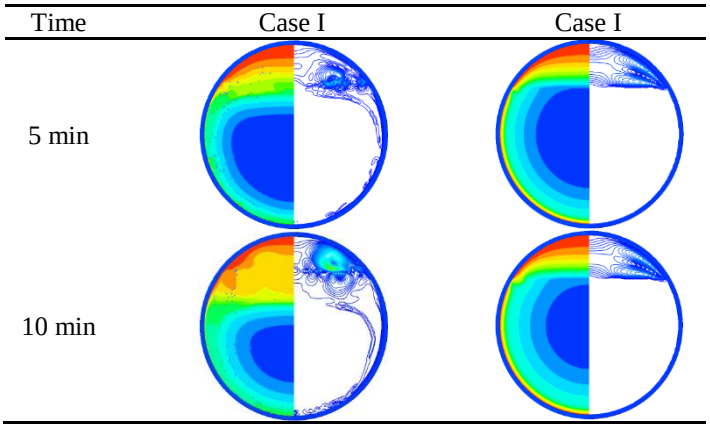

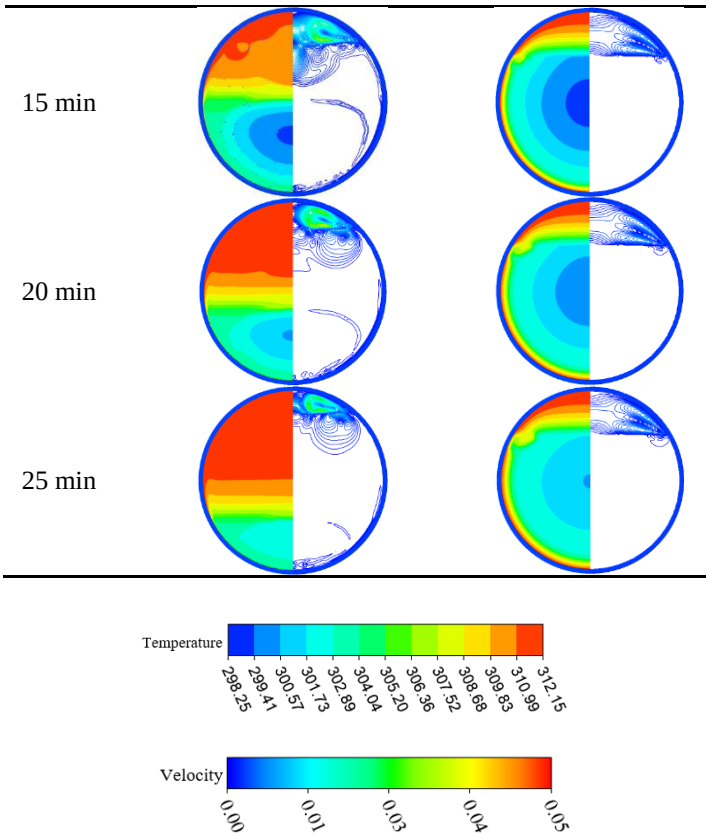

FIGURE 5: COMPOSITE DIAGRAMS FOR DIFFERENT CASES

6. CONCLUSION

Here, unconstrained and constrained melting of PCM is numerically investigated for same volume of PCM and initial and boundary conditions. CFD Fluent 19.2 is used for the investigation. Melt fraction, melting pattern and time are reported. Also, temperature and velocity contours are shown using composite diagrams in this study. It has been reported that the melting is conduction dominated in unconstrained melting, while it is convection dominated in constrained melting at the bottom of the capsule. Melting rate is slower in constrained melting compared to unconstrained melting with complete melting time of 32 min and 220 mins, respectively. Also, unconstrained melting can be more closely simulated numerically to real melting problem with linear density variation compared to constrained melting with Boussinesq approximation.

ACKNOWLEDGEMENT

This work is financially supported by Science Engineering and Research Board (SERB), India under Overseas Visiting Doctoral Fellowship (SBS9Z-032017-XXIV 2018-19) and Department of Science and Technology (DST), India under DST-Inspire fellowship (IF170534).

REFERENCES

[1] E. Assis, L. Katsman, G. Ziskind, R. Letan, Numerical

and experimental study of melting in a spherical shell, Int. J. Heat Mass Transf. 50 (2007) 1790–1804
[2] F.L. Tan, Constrained and unconstrained melting inside a sphere, Int. Commun. Heat Mass Transf. 35 (2008) 466–475
[3] M.Z.M. Rizan, F.L. Tan, C.P. Tso, An experimental study of n-octadecane melting inside a sphere subjected to constant heat rate at surface, Int. Comm. Heat Mass Transf. 39 (2012) 1624–1630
[4] S.F. Hosseinizadeh, A.A.R. Darzi, F.L. Tan, J.M. Khodadadi, Unconstrained melting inside a sphere, Int. J. Therm. Sci. 63 (2013) 55–64
[5] A.R. Archibold, M.M. Rahman, D.Y. Goswami, E.K. Stefanakos, Analysis of heat transfer and fluid flow during melting inside a spherical container for thermal energy storage, Appl. Therm. Eng. 64 (2014) 396–407
[6] A.R. Archibold, J. Gonzalez-Aguilar, M.M. Rahman, D. Yogi Goswami, M. Romero, E.K. Stefanakos, The melting process of storage materials with relatively high phase change temperatures in partially filled spherical shells, Appl. Energy 116 (2014) 243–252
[7] A.F. Elmozughi, L. Solomon, A. Oztekin, S. Neti, Encapsulated phase change material for high temperature thermal energy storage–heat transfer analysis, Int. J. Heat Mass Transf. 78 (2014) 1135–1144
[8] J.F.R. Junior, R.D.C. Oliveski, L.A.O. Rocha, C. Biserni, Numerical investigation on phase change material (PCM): The melting process of erythritol in spheres under different thermal conditions, Int. J. Mech. Sci. 148 (2018) 20-30.
[9] S.T. Revankar, T. Croy, Visualization study of the shrinkage void distribution in thermal energy storage capsules of different geometry, Exp. Therm. Fluid Sci. 31 (2007) 181–189
[10] J.M. Khodadadi, Y. Zhang, Effects of buoyancy-driven convection on melting within spherical containers, Int. J. Heat Mass Transf. 44 (2001) 1605–1618.
[11] F.L. Tan, S.F. Hosseinizadeh, J.M. Khodadadi, L. Fan, Experimental and computational study of constrained melting of phase change materials (PCM) inside a spherical capsule, Int. J. Heat Mass Transf. 52 (2009) 3464–3472.
[12] M. Bechiri, K. Mansouri, S. Saleem, Study of heat sink effects during melting of constrained phase change material inside a spherical enclosure, J. Energy Storage 27 (2020) 101151.
[13] W. Li, S. Li, S. Guan, Y. Wang, X. Zhang, X. Liu, Numerical study on melt fraction during melting of phase change material inside a sphere, Int. J. Hydrogen Ener. 42 (2017) 18232–18239.
[14] L. Fan, Z. Zhu, S. Xiao, M. Liu, H. Lu, Y. Zeng, Z. Yu, K. Cen, An experimental and numerical investigation of constrained melting heat transfer of a phase change material in a circumferentially finned spherical capsule for thermal energy storage, App. Therm. Eng. 100 (2016) 1063-1075.
[15] H. Sattari, A. Mohebbi, M.M. Afsahi, A.A. Yancheshme, CFD simulation of melting process of phase change materials (PCMs) in a spherical capsule, Int. J. Refrig. 73 (2017) 209-218.
[16] R. Kothari, S.K. Sahu, S.I. Kundalwal, Comprehensive analysis of melting and solidification of a phase change material in an annulus, Heat Mass Transf. 55 (2019) 769–790.
[17] R. Kothari, S. Das, S.K. Sahu, S.I. Kundalwal, Analysis of solidification in a finite PCM storage with internal fins by employing heat balance integral method, Int. J. Energy Research 43 (12), 6366-6388.
[18] V.R. Voller, C. Prakash, A fixed grid numerical modelling methodology for convection-diffusion mushy region phase-change problems, Int. J. Heat Mass Transfer 30(8) (1987) 1709-1719.
[19] A.D. Brent, V.R. Voller, K.T.J. Reid, Enthalpy-porosity technique for modelling convection-diffusion phase change: application to the melting of pure metal, Num. Heat Transf. A Appl. 13(3) (1988) 297-318.
[20] S.V. Patankar, Numerical heat transfer and fluid flow, Washington DC, USA: Hemisphere (1980).